

Cosmology of inevitable flat space

Farid Abrari

1400 Woodeden Dr, Mississauga, Ont, L5H 2T9, Canada

farid.abrari@gmail.com

July 3, 2022

Abstract

In the combined theory of Special Relativity and Quantum Mechanics (c-SRQM), the upper limit of local acceleration is constrained to c^2/A , where c is the speed of light and A is the diameter of the event horizon of the *smallest* black hole in nature - called the Unit Black Hole (UBH). In this article, a new cosmological model is proposed wherein the flatness of the universe is inevitable from the onset. The theory indicates that at any given moment of the cosmic evolution, the age of the universe can be expressed as some integer multiple of the *cosmological time constant* A/c . The integer multiple 1, signifies the *end* of the Big Bang at which the initial conditions undergo a sudden change. The *known* universe is then shown to be the *observable* portion of a much bigger structure - named *the grand universe* - which is originated from a Primordial Black Hole (PBH) expanding with the *limit rate* c^2/A at time A/c . It is shown that the dipole in the Cosmic Microwave Background (CMB) could be explained by the anisotropy in the gravitational redshift of the grand universe. Moreover, a best fit to the observational Hubble diagram is obtained when the absolute luminosity of type Ia supernovae is constrained to $3.02e9$ times that of the sun. The age of the universe is found to be $15.96e9$ (years). The new age is higher than that of the standard cosmology by $2.14e9$ (years), therefore, reducing the age discrepancy between the universe and the old metal-deficient stars. The actual value of the Hubble constant H_o is found to be 40.83 (km/sec/Mpc). The discrepancy with the current estimates of the constant is due to neglecting the gravitational redshift of the grand universe in the current standard cosmology.

Keywords — c-SRQM theory, Fine tuning, Multiverse, Black Hole, Big Bang, Hubble constant

1 Background

In the c-SRQM theory, the *local* acceleration is shown to have a physical upper limit given by [1]:

$$a_u = \frac{c^2}{A} \quad (1)$$

where $A = h/\bar{m}c$ is the Compton wavelength of a reference particle with rest mass \bar{m} . The reference particle represents *a particle whose rest mass \bar{m} is the smallest non-zero mass physically possible*. The numerical value of \bar{m} , therefore, is considered to be the cut-off limit of the *massless* particles, i.e. $\{m = 0 | m < \bar{m}\}$. An attempt was made in [26] to constrain \bar{m} ; hence A . The local acceleration limit a_u , moreover, was shown to be the gravitational field strength at the event horizon of all black

holes. The latter was then used to constrain the mass of the *smallest* possible black hole in nature (the least massive), called a Unit Black Hole (UBH), to:

$$M_0 = \frac{Ac^2}{4G} \quad (2)$$

and further constrain the diameter of its event horizon to A . Not having a point-like *mathematical* singularity of zero volume (and hence, infinite mass density), the event horizon of the UBH was shown to represent the boundary of the *physical* singularity; constraining the mass density of singularity ρ_s to the limit:

$$\rho_s = \frac{3}{2\pi} \left(\frac{l_p}{A}\right)^2 \rho_p \quad (3)$$

where $l_p = \sqrt{G\hbar/c^3}$ is the Planck length and $\rho_p = c^5/G^2\hbar$ is the Planck density. Subsequently, the mass M_b , event horizon diameter D_b and temperature T_b of black holes were quantized as [1]:

$$\begin{aligned} M_b &= M_0 + \frac{1}{4} b m_p \\ D_b &= A + b l_p \\ T_b &= \frac{l_p}{2\pi D_b} T_p \end{aligned} \quad (4)$$

where $m_p = \sqrt{\hbar c/G}$ is the Planck mass, $T_p = m_p c^2/\kappa$ is Planck temperature, κ is the Boltzmann constant and $b = 0, 1, 2, \dots$ is the *quantum index of black holes*. It was also noted that the temperature equation above was the quantized form of Hawking radiation [11]:

$$T = \frac{\hbar c^3}{8\pi G M \kappa} \quad (5)$$

As shown in Fig 1, the diameter of the event horizon of black holes increase by one Planck length for every unit increase of the quantum index b . It is evident that the lowest quantum index $b = 0$ corresponds to the smallest black hole in nature. Since the mass density of the UBH singularity is at the physical limit ρ_s , any additional mass added to the UBH towards generating a more massive black hole (i.e. the term $\frac{1}{4} b m_p$ in Eqn 4) can only be accumulated *outside* of the UBH singularity. This generates the *core* of more massive black holes. This article begins with the

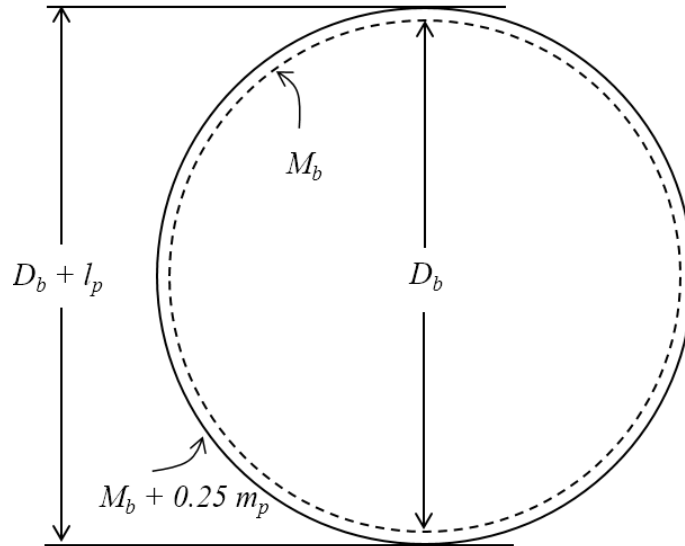


Figure 1: The diameter of the event horizon increases by one l_p for every $0.25m_p$ mass added assumption that the black hole quantum index b has an upper limit beyond which a super massive

black would become unstable. The physics of such behaviour is of course not known today. Based on this assumption, however, a matter-dominated (Einstein-de Sitter) model of a grand universe is introduced which begins when the core of a super massive primordial black hole gets unstable. The known universe is then shown to be a small observable portion of a much bigger grand universe. It is further shown that by taking the gravitational redshifts of the grand universe into account (one can say, gravitational redshift of a matter which is missing from the observations), the resulting decelerating model of the universe fits the observed Cosmological Microwave Background (CMB) dipole and type Ia Supernovae data rather well. Due to its simplicity and intuitive nature, the Newtonian approach is used to solve the expansion of the PBH core using a set of initial conditions. An accurate solution can only be obtained considering the relativistic aspects. The author hopes this article inspires a General Relativistic solution to the proposed initial value problem in the future.

2 Initial conditions at Big Bang

As illustrated in Fig 2, consider a *spherical shell* of thickness dR and mass dm on a sphere of radius R and mass m , concentric with the PBH core. A more formal definition of the core of a Black Hole will come in the following section. In principle, each shell of mass dm within the PBH core, at *any* given instant in time has a coordinate exclusive to itself. We call this the principle of *exclusive coordinates*. For the mass m of the sphere R we can now write:

$$m = \frac{4}{3}\pi R^3 \rho_m(0^+, R) \quad (6)$$

where $\rho_m(0^+, R)$ is the *mass density distribution* within the PBH core when the universe is only one cosmological time-step old, i.e at time $0^+ = A/c$. The instant signifies the end of the Big Bang. As will be revealed later, the density is constant and equal to ρ_s , but for now it is written as a function R . The equation of motion of the shell R under the sole influence of gravity is then given by:

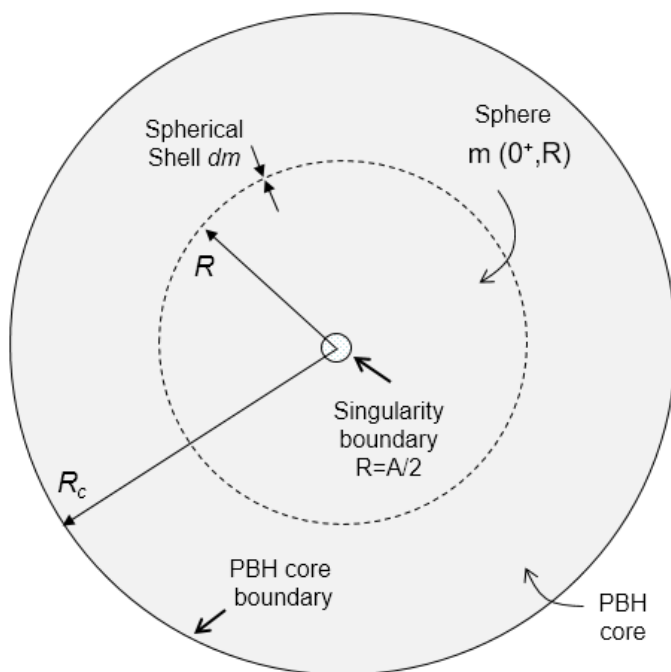


Figure 2: Galaxies originating from a PBH shell have common comoving coordinates

$$\ddot{r} + \frac{4}{3}\pi \frac{GR^3}{r^2} \rho_m(0^+, R) = 0 \quad (7)$$

where $r(t, R)$ is the radial coordinate of shell R versus cosmic time t any time after the Big Bang. A detailed review of solution to such matter dominated model can be found in [3]. Substituting the *dimensionless scale factor*:

$$a = r/R \quad (8)$$

and its second derivative $\ddot{a} = \ddot{r}/R$ in Eqn 7 we arrive at:

$$\ddot{a} + \frac{4}{3}\pi\frac{G}{a^2}\rho_m(0^+, R) = 0 \quad (9)$$

Evidently, the *steady state condition* of the PBH core prior to the Big Bang, at time $0 < A/c$, is given by:

$$\begin{aligned} a(0) &= \frac{R}{R} = 1 \\ \dot{a}(0) &= 0 \end{aligned} \quad (10)$$

We now hypothesize that the initial conditions of the PBH at time $0^+ = A/c$ is:

$$\begin{aligned} a(0^+) &= \frac{R}{R} = 1 \\ \dot{a}(0^+) &= \frac{2}{A}c \end{aligned} \quad (11)$$

The initial conditions for the radial coordinate r can then be easily obtained from Eqn 11 as follows:

$$\begin{aligned} r(0^+, R) &= R \\ \dot{r}(0^+, R) &= \frac{2R}{A}c \end{aligned} \quad (12)$$

Multiplying Eqn 9 by the *integrator* \dot{a} we get:

$$\dot{a}[\ddot{a} + \frac{4}{3}\pi\frac{G}{a^2(t)}\rho_m(0^+, R)] = \frac{dE}{dt} = 0 \quad (13)$$

where:

$$E = \frac{1}{2}\dot{a}^2 - \frac{4}{3}\pi G\frac{1}{a}\rho_m(0^+, R) \quad (14)$$

For a matter dominated flat universe we have the constraint $E = 0$ [3]. From Eqn 14, we then have:

$$\dot{a}^2(t) = \frac{8}{3}\pi G\frac{1}{a(t)}\rho_m(0^+, R) \quad (15)$$

Substituting for the initial conditions $a(0^+)$ and $\dot{a}(0^+)$ from Eqn 11 in above we verify that the mass density distribution in the PBH at the onset of Big Bang is uniform and equal to that of the singularity, i.e. not a function of comoving coordinate R . Therefore, we now drop the variable R from the equation of density to arrive at:

$$\rho_m(0^+) = \frac{3c^2}{2\pi GA^2} = \rho_s \quad (16)$$

This further confirms that to respect the limit density of Eqn 3, the shells within the core cannot cross each other at the onset of Big Bang; nor can they can be compressed to each other - as satisfied by the initial conditions of Eqn 12. Denoting the PBH mass M_{gu} as the mass of the grand universe, then PBH core radius R_c can be determined from the integral:

$$M_{gu} - M_0 = \int_{A/2}^{R_c} 4\pi R^2 \rho_m(0^+) dR \quad (17)$$

The distance between the boundaries of the singularity and the core, i.e span $R_c - A/2$, hence, represents the entire range of *comoving coordinates* that have been expanding since the Big Bang. Substituting for the density distribution from Eqn 16 and integrating Eqn 17 we finally arrive at the following for the radius of the core of the PBH as:

$$R_c = \left(\frac{M_{gu}}{M_0}\right)^{\frac{1}{3}} \frac{A}{2} \quad (18)$$

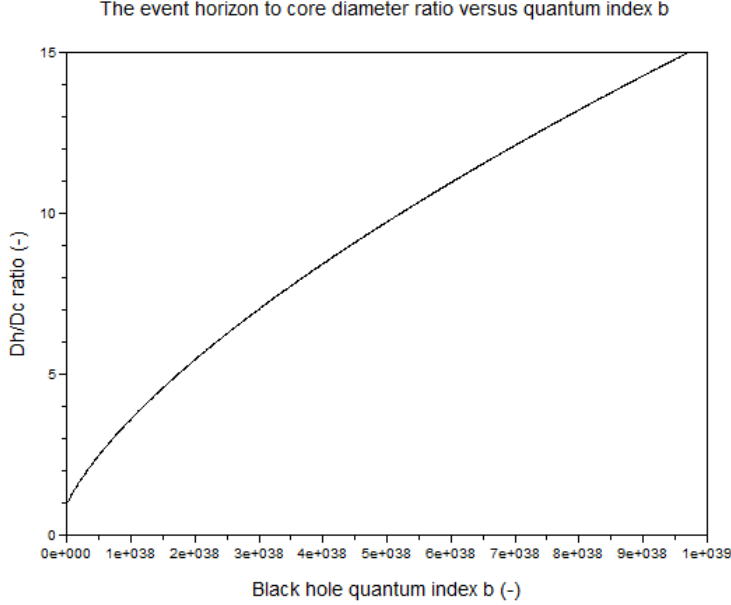


Figure 3: Ratio of event horizon to core diameter versus black hole quantum index b

3 Core of black holes

We shall now generalize the definition of the core of a black hole as *a limit radius inside a black hole beyond which there is no matter concentration*. From Schwarzschild equation [9] we have:

$$M_{gu} = \frac{R_h c^2}{2G} \quad (19)$$

where R_h is the event horizon of the PBH. In Eqn 18, by substituting for M_{gu} from Eqn 19 we then have the following relation between the diameters of the core D_c and event horizon D_h of the PBH (and infact for all black holes in general):

$$D_c = \left(\frac{D_h}{A}\right)^{\frac{1}{3}} A \quad (20)$$

Since the condition $\frac{D_h}{A} > 1$ is true for all black holes that are more massive than the UBH, then from Eqn 20, the condition $D_c < D_h$ is also true for all black holes. This is as expected, since by the very definition of black holes, *the core must always be engulfed by the event horizon*. Furthermore, note that for the UBH with the event horizon $D_h = A$, from Eqn 20 we then have $D_c = D_h = A$; meaning that *the singularity, the core, and the event horizon of the unit black hole all coincide* at diameter A , a feature uniquely valid for the UBH. Fig 3, shows the ratio of D_h/D_c versus quantum index b of black holes.

4 Scale factor of the expanding universe

Now, by substituting for the initial density distribution from Eqn 16 in Eqn 15 we arrive at:

$$\int_1^{a(t)} \sqrt{a} da = \frac{2c}{A} \int_{A/c}^t dt \quad (21)$$

And by integrating above we finally have the equation of scale factor a versus cosmic time t :

$$a(t) = \left[\frac{3}{A}(ct - A) + 1 \right]^{\frac{2}{3}} \quad (22)$$

Fig 4 shows evolution of the scale factor in terms of cosmological timestep A/c after the Big Bang. The equation of scale factor $a(t)$ not being a function of comoving coordinate R indicates the model

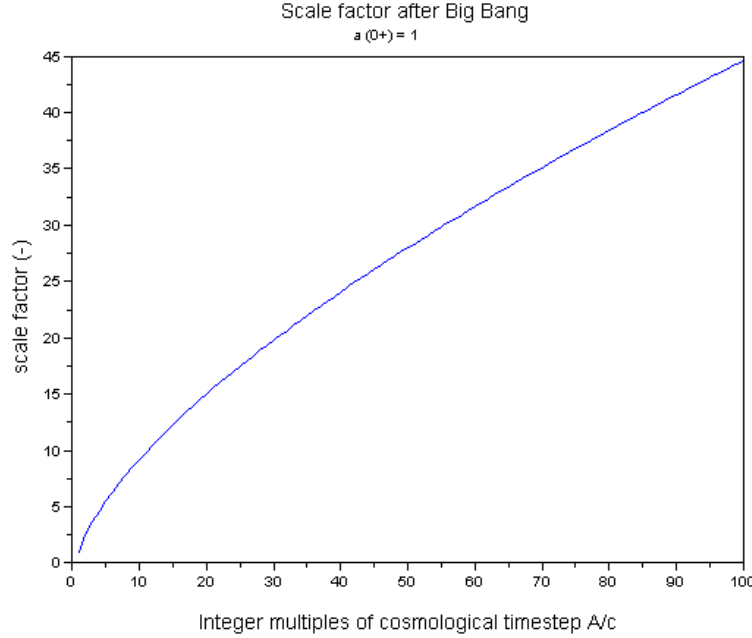


Figure 4: Evolution of scale factor starting from initial value 1 at Big Bang

represents an *isotropic expansion* of the universe. Also, note that at the Big Bang $0^+ = A/c$, from the equation we have $a(0^+) = 1$, as expected from the imposed initial conditions. Taking the derivative of Eqn 22 we then have the following for the time evolution of scale factor:

$$\dot{a}(t) = \frac{2c}{A} \left[\frac{3}{A}(ct - A) + 1 \right]^{-\frac{1}{3}} \quad (23)$$

Note again that at the Big Bang $0^+ = A/c$ from Eqn 23 we have:

$$\dot{a}(0^+) = \frac{2}{A}c \quad (24)$$

as expected from the imposed velocity initial condition. Fig 5 shows evolution of the scale factor in terms of cosmological timestep A/c after the Big Bang. Taking the second derivative of Eqn 22 we will have:

$$\ddot{a}(t) = -\frac{2c^2}{A^2} \left[\frac{3}{A}(ct - A) + 1 \right]^{-\frac{4}{3}} \quad (25)$$

Note again that at Big Bang $0^+ = A/c$ from Eqn 25 we have:

$$\ddot{a}(0^+) = -\frac{2c^2}{A^2} = -\frac{2}{A}a_u \quad (26)$$

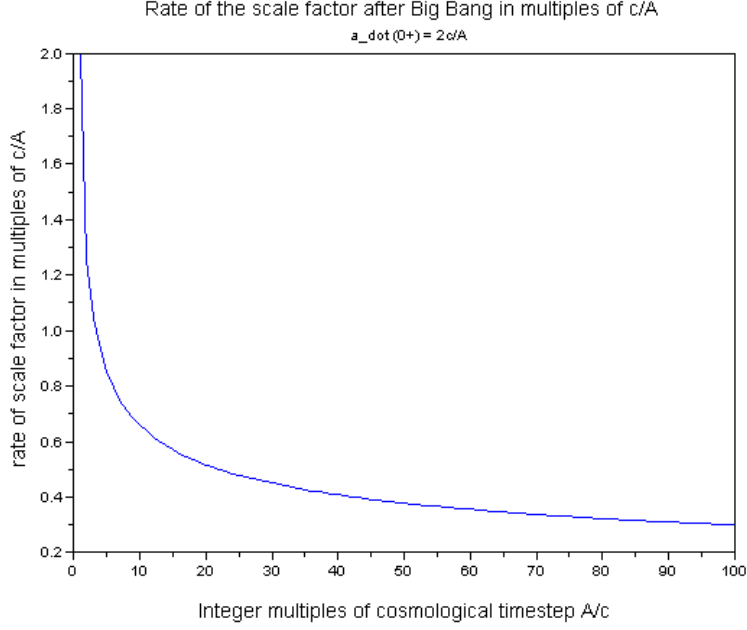


Figure 5: Rate of change of scale factor starting from initial value $2c/A$ at Big Bang

Multiplying each one of the Eqns 22, 23 and 25 by R would give the equations for the radial coordinate, velocity and deceleration of the expanding space (Hubble flow) versus time t :

$$\begin{aligned}
 r(t, R) &= R \left[\frac{3}{A}(ct - A) + 1 \right]^{\frac{2}{3}} & (27) \\
 \dot{r}(t, R) &= \frac{2Rc}{A} \left[\frac{3}{A}(ct - A) + 1 \right]^{-\frac{1}{3}} \\
 \ddot{r}(t, R) &= -\frac{2Rc^2}{A^2} \left[\frac{3}{A}(ct - A) + 1 \right]^{-\frac{4}{3}}
 \end{aligned}$$

Now, note that from the third Eqn in 27 at Big Bang $0^+ = A/c$ we have:

$$\ddot{r}(0^+, R) = -\frac{2R}{A} a_u \quad (28)$$

This condition is directly correspond to the *gravitational field strength* at each shell R inside the PBH, because:

$$g(0^+, R) = -\frac{Gm(0^+, R)}{R^2} = -\frac{4}{3}\pi GR\rho_s \quad (29)$$

But for the limit acceleration a_u we have:

$$a_u = \frac{GM_0}{(\frac{A}{2})^2} = \frac{2}{3}\pi GA\rho_s \quad (30)$$

therefore, comparing Equations 29 and 30 it is evident that:

$$g(0^+, R) = -\frac{2R}{A} a_u \quad (31)$$

which is found to be identical to Eqn 28. Since radius R of shells are measured from the geometric center of the PBH, Eqn 31 represents the *global* expansion rate of the comoving coordinates due to the Big Bang which is found to be equal to the gravitational field strength within the PBH at the Big Bang. Moreover, as a direct consequence of the principle of exclusive coordinates, the mass conservation within a sphere is given by:

$$m(0^+, R) = m(t, r) \quad (32)$$

Eqn 32 indicates that the total mass within a sphere at the current epic radius $r(t, R)$ is equal to the mass that was originally existed in the primordial *sphere* R . From Eqn 32, the temporal density of the universe is therefore given by:

$$\rho_m(t) = \frac{\rho_m(0^+)}{a^3(t)} = \frac{3c^2}{2\pi GA^2} \frac{1}{a^3(t)} \quad (33)$$

5 Spatial expansion redshift

As a light beam travels the distance between the emission and observation points in space, the inner-space between the points continuously increases due to the expansion of space. As a result, the light beam suffers a redshift due to the expansion of the inner-space between the points. The higher the spatial expansion, i.e. the farther the initial distance between the points, the higher the cosmological redshift turns out to be. The spatial redshift z_x is directly related to the ratio of scale factors $a(t)$ as follows:

$$z_x = \frac{a(t_o)}{a(t_e)} - 1 \quad (34)$$

where $a(t_e)$ and $a(t_o)$ are the scale factors at the time of emission t_e and observation t_o of the photon. Fig 6 compares travel of a light beam from one distant galaxy to another (left to right) at *equal time intervals* (top to bottom) in two distinct universes of static and expanding character. In

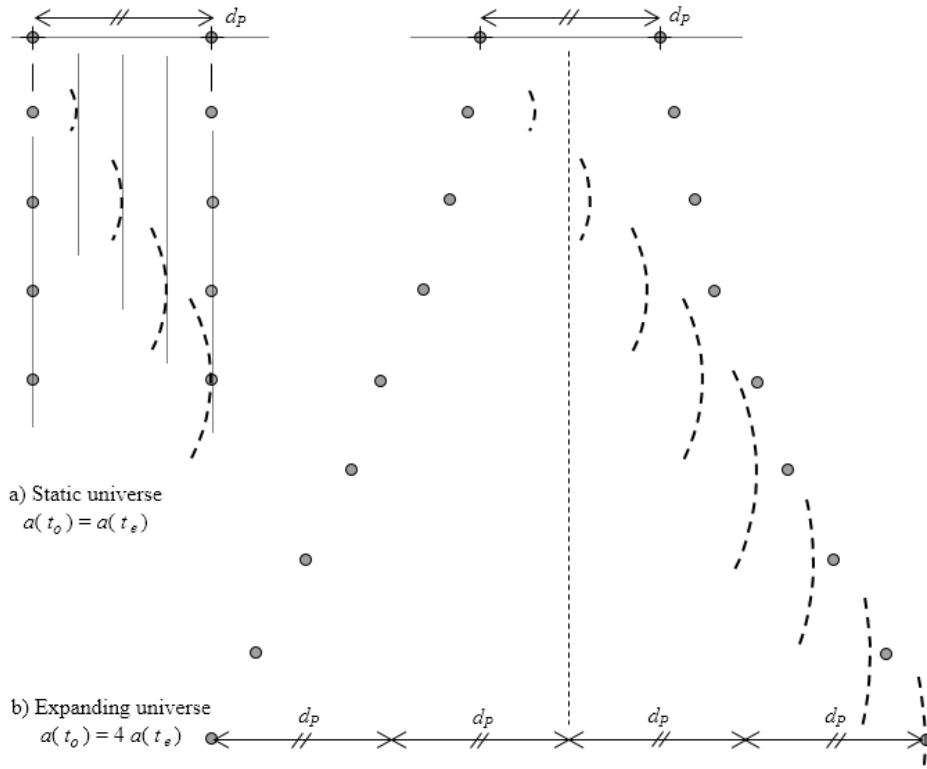


Figure 6: Redshift $z_x = 3$ for galaxies receding with the speed of light

Fig 6a, the universe is assumed to be static, therefore, unlike the case of an expanding universe in Fig 6b, the distance between the galaxies remains constant as light travels from left to right (shown by moving dashed arcs). In this condition, we then have $a(t_o) = a(t_e)$; and with that, from Eqn 34, the spatial redshift corresponding to a static world will be $z_x = 0$; as expected. In Fig 6b, the universe is assumed to be expanding; and moreover, the *initial* proper distance d_p between the galaxies is assumed to be such that the expanding space results in moving the galaxies away from each other with the speed of light c . In this case, immediately after the emission, as the light beam

covers some distance to the right, the galaxies separate from each other by the same amount. But as the distance between galaxies increases with the passage of time, their separation distance during a given time interval dt gets higher than the distance cdt traveled by the light beam. As shown in Fig 6b (top to bottom), it turns out that by the time the light beam eventually arrives at the observing galaxy, the universe expands by a scale factor of 4 in *all* directions. From Eqn 34, the redshift of the light beam upon arriving at the observing galaxy would then be $z_x = 3$ due to the expansion of space alone. As will be discussed in the following section, the *measurable* redshift, however, would be a superposition of the spatial z_x and the gravitational z_g redshifts. Now, consider a pair of galaxies at distances even farther than d_P of our illustration. In that case, their recession velocity would then be even higher than the speed of light c and with that their spatial redshift $z_x > 3$. With increasing d_P , we eventually arrive at a distance where the recession velocity of the galaxies approaches to $2c$. That distance marks the *observable horizon* of the universe. The light emitting from galaxies at such distances would never be able to catch up with the expansion of space; and as a result, they will remain outside of each other's observable horizon. The redshift corresponding to that scenario is $z_x \rightarrow \infty$.

6 Gravitational redshift

The gravitational redshift z_g , is related to the *gravitational potential difference* between the points of emission and observation, as shown in Fig 7. Using the formula of the gravitational potential

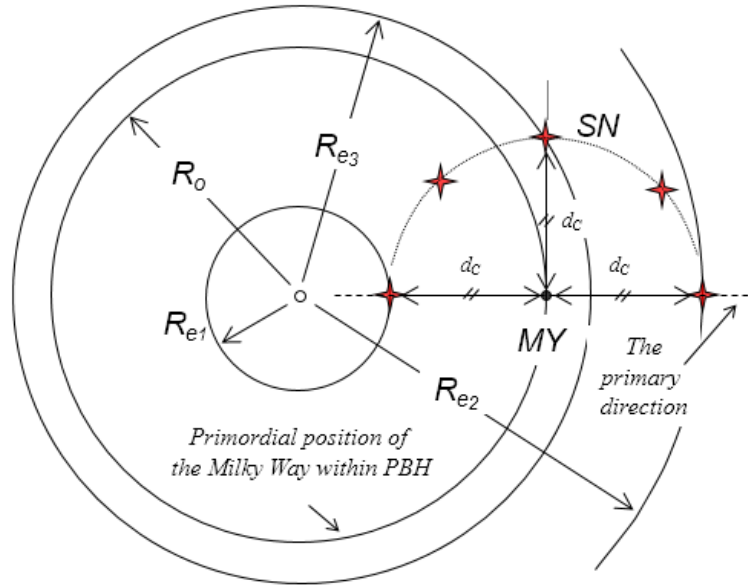


Figure 7: Primordial position of equidistant supernovae relative to the Milky Way

within a sphere [5] - where the contribution of a *spherical mass below* a given radius r is added to that of the *shell mass above* it - the potentials at the emission and observation points can be obtained from:

$$\Phi_o(r, r_c) = -\frac{GM_{gu}}{2r_{co}^3}(3r_{co}^2 - r_o^2) \quad (35)$$

$$\Phi_e(r, r_c) = -\frac{GM_{gu}}{2r_{ce}^3}(3r_{ce}^2 - r_e^2)$$

where $r_e = r(R_e, t_e)$ and $r_o = r(R_o, t_o)$ are the radial coordinates of the emission and observation points, respectively; and $r_{ce} = r(R_c, t_e)$ and $r_{co} = r(R_c, t_o)$ are the radial coordinates of the PBH

core boundary at the corresponding times. From the theory of general relativity, the gravitational redshift is related to these gravitational potentials through the following equation [6]:

$$z_g = \sqrt{\frac{1 + 2\Phi_e}{1 + 2\Phi_o}} - 1 \simeq \sqrt{\frac{\Phi_e}{\Phi_o}} - 1 \quad \dots \text{ for } \Phi \gg 1 \quad (36)$$

The *measurable* redshift from any object, therefore, includes the total effect of *both* the spatial and gravitational redshifts as:

$$z_{xg} = z_x + z_g \quad (37)$$

Now consider a case where multiple supernovae of *identical* absolute luminosities occur *simultaneously* at *equal distances* from the Milky Way, as shown in Fig 7. Note that the simultaneous explosions in this context means the events occur at the *same cosmological time* t_e after the Big Bang. Due to their equal distances and absolute luminosities, it is evident that in this case the supernovae will have equal apparent luminosities. However, according to Eqn 37, due to their different gravitational redshifts, their *measured* redshifts upon arrival to the Milky Way would be different from each other depending on their directions. As will be discussed in the following section, the magnitude of the anisotropy in the measured redshifts is a function of the distances and directions in the sky. A direction along which the redshift anisotropy is *maximum*, herein, is called *the primary direction*.

7 The primary direction - CMB dipole

As discussed above, since the scale factor $a(t)$ is a function of time only, the redshift z_x turns out to be fully *isotropic*. However, since the gravitational potential $\Phi(r, r_c)$ is a function of position, the resulting gravitational redshift z_g turns out to be *anisotropic* in our cosmological model. The standard model of cosmology, in contrast, lacks such a mechanism for generating a universal anisotropy. As a result, the basic means to explain the measured dipole moment of the CMB in the standard model is through the Doppler effect of the local peculiar motion of the Milky Way relative to the CMB frame [12] by $\approx 620\text{km/sec}$. The validity of this interpretation is found debatable, as discussed in [13, 14]. In our cosmological model, a light beam that is traveling in a direction away from the PBH singularity would undergo a higher redshift compared to a light beam that is traveling towards the singularity. The resulting anisotropy, therefore, provides universal mechanism for the origin of the CMB dipole moment. Accordingly, for the total redshift of the CMB at the poles, which correspond to the maximum redshift anisotropy, we write:

$$\begin{aligned} z_x + z_{g_+} &= \frac{T_{rec}}{T_o - \Delta T} - 1 \\ z_x + z_{g_-} &= \frac{T_{rec}}{T_o + \Delta T} - 1 \end{aligned} \quad (38)$$

where T_{rec} is the temperature of the universe at the time of recombination, i.e. photon decoupling from the *Last Scattering Surface* (LSS), z_{g_+} is the gravitational redshift of the light *moving away* from the singularity (therefore, generating a pole ΔT *colder* than the mean CMB temperature T_o) and z_{g_-} is the gravitational redshift of the light *moving toward* the singularity (therefore, generating a pole ΔT *hotter* than the mean CMB temperature T_o). Subtracting the second equation from the first one, we then arrive at a constraining equation on the gravitational redshift anisotropy required for the CMB dipole of amplitude ΔT and mean T_o , under recombination temperature T_{rec} :

$$g_{z_+} - g_{z_-} = \frac{2 T_{rec} \Delta T}{T_o^2 - \Delta T^2} \quad (39)$$

According to Eqn 39, since the maximum gravitational anisotropy is achieved along the light path connecting the CMB poles, therefore, the latter is considered as the primary direction in our cosmological model. In other words, the primary direction in the sky (i.e. the *radial Hubble flow direction*)

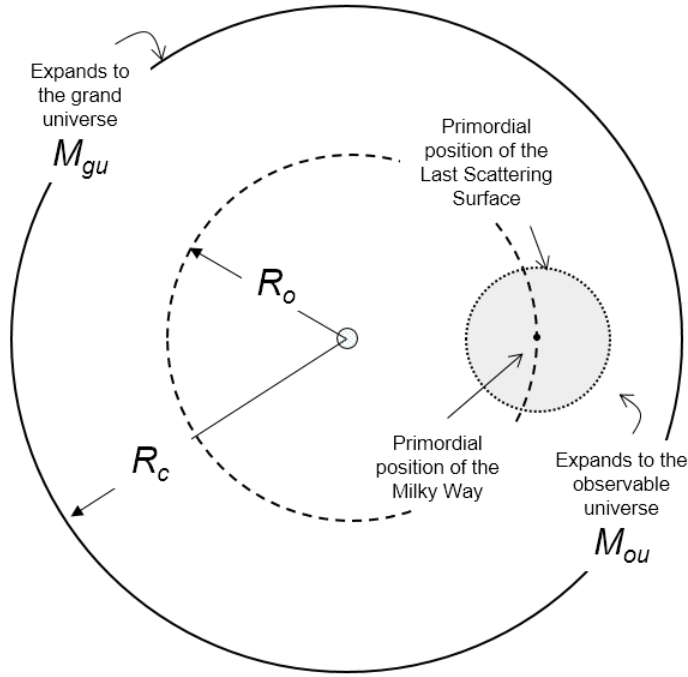


Figure 8: Primordial position of the Milky Way and LSS in the PBH core

is along a direction that connects the constellation Aquarius (cold CMB Pole) to the constellation Leo (hot CMB Pole) through the Milky Way.

8 Numerical simulation - CMB dipole

The primordial position of the LSS and the Milky Way, at the center of it, is illustrated in Fig 8. The LSS is taken to be at a distance from the Milky Way that is close to the ultimate horizon of the observable universe. The latter is assumed to be *fully inside* the grand universe, therefore, homogeneous in all directions. The overall steps required for the numerical simulation of the CMB dipole is illustrated in Fig 9a-c. The comoving coordinate R_o of the Milky Way is shown in Fig 9a

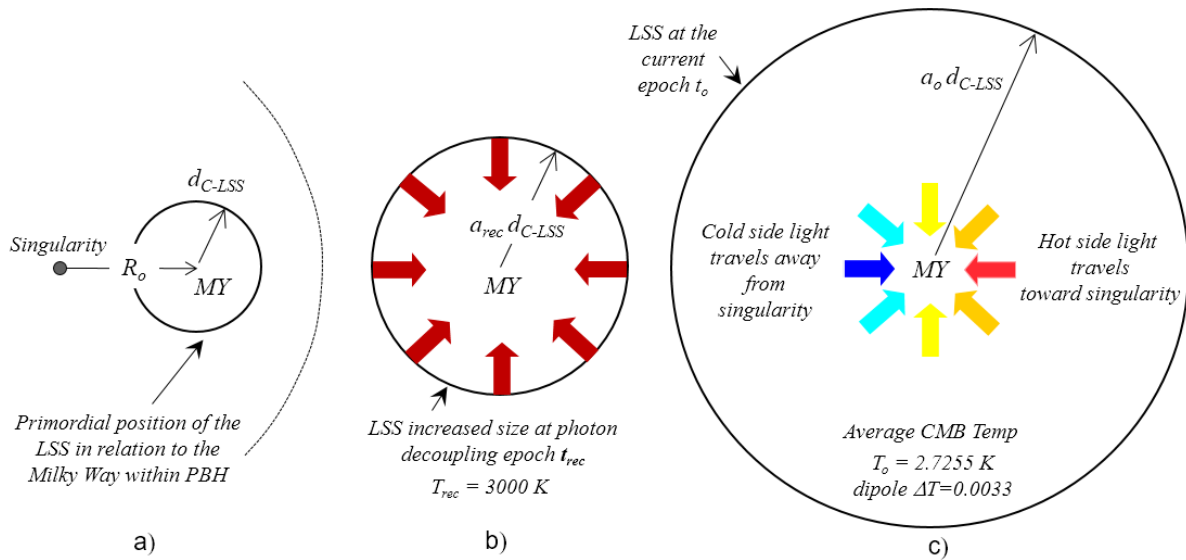


Figure 9: Gravitational potential of grand universe leading to the CMB temperature dipole

in relation to the LSS of comoving radius d_{C_LSS} . Fig 9b, shows the universe expansion to the scale factor a_{rec} at the time t_{rec} when, upon photon decoupling, beams of light are free to scatter from the LSS which now has the radius of $a_{rec} \times d_{C_LSS}$. As the light travels away from the points of emission, as shown in Fig 9c, the universe continues expanding to the scale factor a_o at the current epoch t_o when the light finally arrives at the Milky Way from different directions. A light beam that has been ascending away from the PBH singularity (i.e. coming from the direction of Aquarius constellation) undergoes more redshift compared to the light beam that has been descending towards it (i.e. coming from the direction of Leo constellation). This leads to a redshift anisotropy that peaks at the CMB dipole. Taking the CMB mean temperature of $T_o = 2.7255$ (K), dipole amplitude of $\Delta T = 0.00335$ (K) and recombination epoch temperature of $T_{rec} = 3000$ (K) the gravitational redshift anisotropy that needs to be satisfied in the numerical simulation is obtained from Eqn 39 as $g_{z+} - g_{z-} = 2.70585(-)$. The main independent parameter in the simulation of the CMB dipole is the mass ratio M_{gu}/M_{ou} . The remaining model parameters, i.e. current epoch t_o , recombination epoch t_{rec} , comoving distance d_{C_LSS} , comoving coordinates R_{e_LSS} of the emission points on the LSS and the relative position of the Milky Way within the PBH, i.e the ratio R_o/R_c , are found iteratively such that the final back-calculated M_{gu}/M_{ou} ratio is in agreement with the initially assumed value while the maximum gravitational redshift anisotropy of 2.70585 is also satisfied along the primary direction.

Note that the CMB satellites (COBE, WMAP and Planck) all measure the background microwave radiation in relation to the galactic coordinate system (l, b) , in which the *galactic plane* - containing the Sagittarius A* and the sun - is located at the zero latitude $b = 0$ and the ray connecting the sun to the center of galaxy is located at the zero longitude $l = 0$. It is now important to note that the galactic plane can only have 3 distinct orientations in relation to the primary direction; namely, be either perpendicular, parallel or at an angle relative to the primary direction in the sky, as shown in Fig 10. If the galactic plane were to be perpendicular to the primary direc-

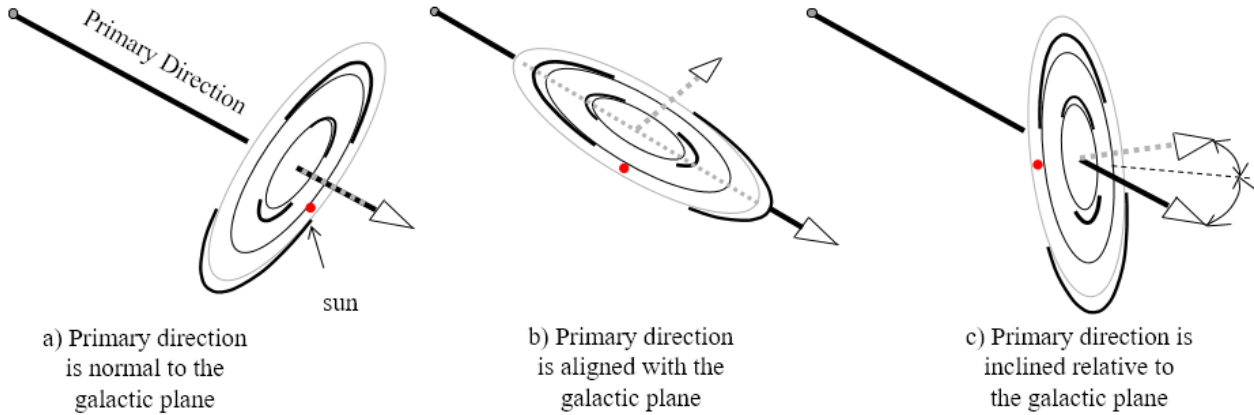


Figure 10: Galactic plane orientation in relation to the primary direction

tion, as shown in Fig 10a, then the hot and cold poles (which are always aligned with the primary direction) would have been located exactly at the north and south poles ($b = \pm 90^\circ$) of the galactic coordinate system, respectively. This is exactly what is shown in Fig 11 where the CMB dipole are at galactic poles. On the other hand, if the galactic plane were to be parallel to the primary direction, as shown in Fig 10b, then the hot and cold poles would have been located exactly at the equator ($b = 0^\circ$) of the galactic coordinate system, as shown in Fig 12. In this plot, the ray from the sun to the Sagittarius A* is set at zero longitude, therefore, the CMB dipoles are located at $\pm 90^\circ$ longitude. Finally, if the north pole of the galactic coordinate system were to be rotated by $(l, b) = (264^\circ, 48.26^\circ)$, i.e. in line with the actual location of the measured CMB dipoles, then the CMB dipole in the model universe would be seen as shown in Fig 13, closely resembling to the

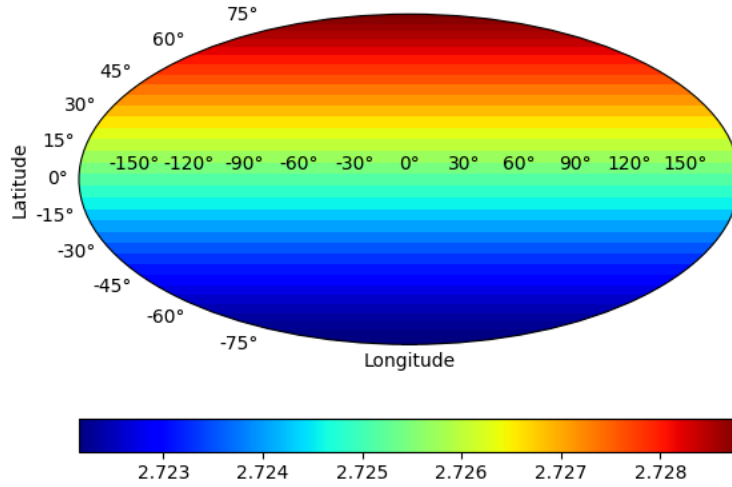


Figure 11: CMB dipole if galactic plane was perpendicular to the primary direction

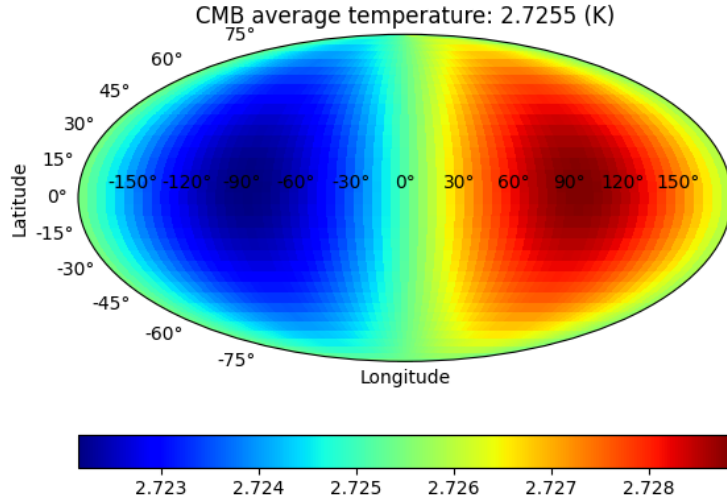


Figure 12: CMB dipole if galactic plane was parallel to the primary direction

actual CMB measured by COBE satellite shown in Fig 14. Note that the CMB mean, amplitude ΔT of the dipole and the overall pattern of the model universe matches the actual data rather well. In the numerical simulation of CMB dipole, first a sphere of radius d_{C_LSS} is generated such that it is initially concentric with the PBH singularity and its north pole is along the primary direction. The surface of the sphere is then digitized using a grid of $5^\circ \times 5^\circ$ patch. In total, therefore, we have $360/5 = 72$ points on the longitudinal direction, $90/5 = 18$ points on the positive latitude side (towards North Pole) and 18 points on the negative latitude side (towards South Pole). The original coordinates of each point on the grid is then calculated from:

$$\begin{bmatrix} P''_x \\ P''_y \\ P''_z \end{bmatrix} = d_{C_LSS} \begin{bmatrix} \cos(\phi) \cos(\theta) \\ \cos(\phi) \sin(\theta) \\ \sin(\theta) \end{bmatrix} \quad (40)$$

where θ is the latitude and ϕ the longitude angle of a given point on the grid. Then to align the coordinate system with the dipole coordinates $(l, b) = (264^\circ, 48.26^\circ)$, we first rotate the original coordinate system about its z-axis by $l = 264^\circ$ followed by a rotation about, now, the rotated y'-axis by $b = 48.26^\circ$. The grid coordinates are therefore transformed from the original frame above

to the rotated one as follows:

$$\begin{bmatrix} P'_x \\ P'_y \\ P'_z \end{bmatrix} = \begin{bmatrix} \sin(b) \cos(l) & \sin(b) \sin(l) & -\cos(b) \\ -\sin(l) & \cos(l) & 0 \\ \cos(b) \cos(l) & \cos(b) \sin(l) & \sin(b) \end{bmatrix} \begin{bmatrix} P''_x \\ P''_y \\ P''_z \end{bmatrix} \quad (41)$$

The origin of the sphere is then finally transformed from the center of PBH to the radial position

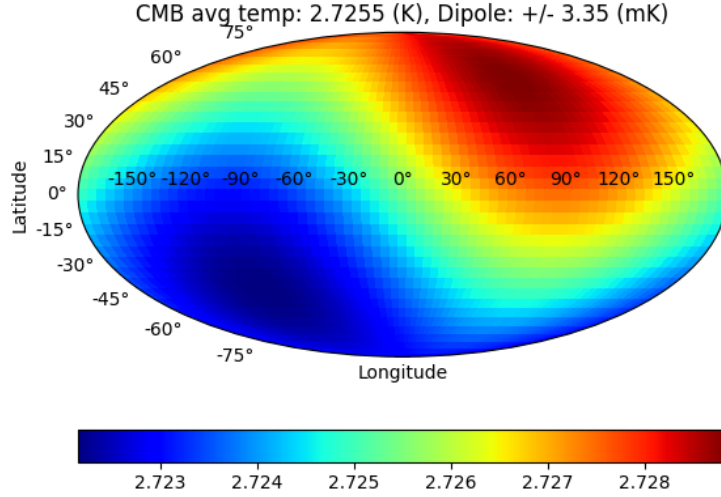


Figure 13: CMB dipole if galactic plane was inclined relative to the primary direction

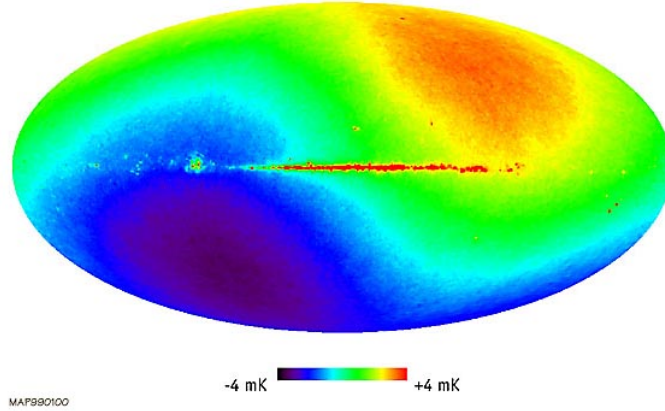


Figure 14: CMB dipole from COBE [15]

R_o of the Milky Way using the following transform:

$$\begin{bmatrix} P_x \\ P_y \\ P_z \end{bmatrix} = \begin{bmatrix} P'_x + R_o \\ P'_y \\ P'_z \end{bmatrix} \quad (42)$$

From the last equation, the primordial comoving coordinate of the emission points (i.e. grid points) on the LSS is therefore obtained from:

$$R_{e_LSS} = \sqrt{P_x^2 + P_y^2 + P_z^2} \quad (43)$$

Before concluding this section, let's remark here that neither the mass M_{gu} of the grand universe nor the primordial position R_o of the Milky Way, can be constrained using the CMB dipole alone.

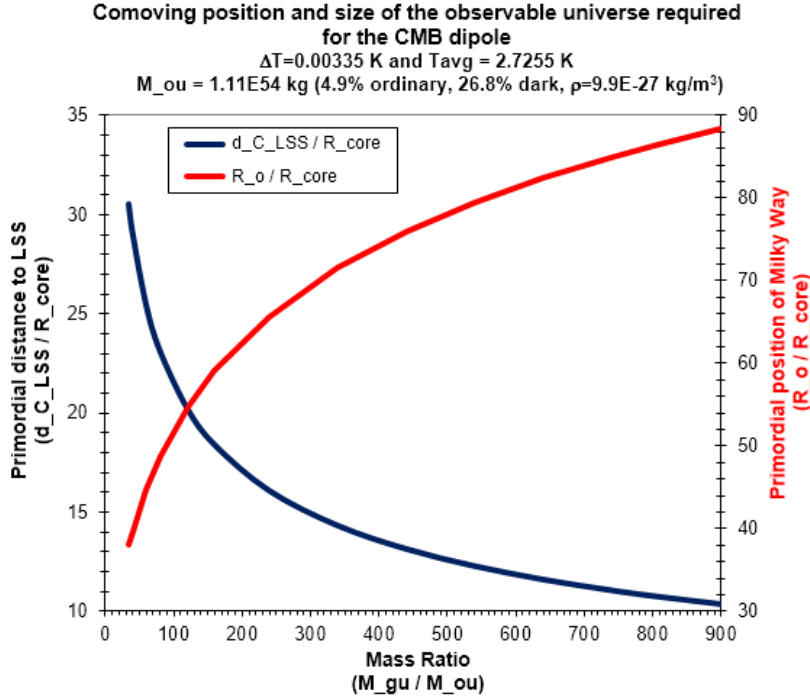


Figure 15: Model parameters supporting measured CMB dipole

The reason is that all combinations of the M_{gu} and R_o parameters that result in a matching CMB dipole also produce numerically identical CMB temperature distribution across the sky, leaving no discriminating features to constrain the model parameters. Whether a much finer numerical simulation, or a solution based on General Relativity can alter this conclusion is yet to be seen in the future. The numerical simulations, nonetheless, constrain the grand universe mass ratio to the range $\sim 35 < M_{gu}/M_{ou} < \sim 900$. Since the proposed model is a matter-dominated, Einstein-de Sitter type universe [25], in the estimation of M_{ou} we have considered only the ordinary plus the dark matter amounting to $4.9\% + 26.8\% = 31.7\%$ of the total density $9.9e-27 \text{ (kg/m}^3)$ [23]. It turns out that under $M_{ou} \sim 1.11e54 \text{ (kg)}$, comprising the ordinary plus the dark matter, a consistent solution could be obtained permitting the observed CMB dipole as discussed before. The constrain on the remaining parameters R_o and d_{C_LSS} is shown in Fig 15. It is noted that the more massive the grand universe M_{gu} is, the more outwardly must be the position of the observable universe within it. Using the range of permissible M_{gu} , the steady state PBH core temperature prior to the Big Bang is constrained by Eqn 5 to the range $31.5e-34 \text{ (K)} > T_{core_initial} > 1.2e-34 \text{ (K)}$. The temperature, immediately after the Big Bang, $T_{BB} \sim 2.13e16 \text{ (K)}$ is calculated knowing both the a_{rec} and $T_{rec} = 3000 \text{ (K)}$ and the fact that $a_{0+} = 1$. The proper distance to LSS is found to be $\sim 14200 \text{ (Mpc)}$, resulting the observable universe of diameter $92.8e9 \text{ (Ly)}$.

The age of the universe and the recombination time are found to be $15.96e9$ and 456600 (years) . From Eqn 33, the current epoch mass density $\rho_s/a_o^3 = 3.137e-27 \text{ (kg/m}^3)$, which is exactly 31.7% of the total density $9.9e-27 \text{ (kg/m}^3)$ (due to the exclusion of the dark energy - as discussed above). Compared to the current estimation of the recombination time from the standard model $t_{rec_standard} = 378000 \text{ (years)}$, photon decoupling is delayed by 78600 (years) in our model. Also, compared to the current estimate of the universe age from the standard cosmology, $t_{o_standard} = 13.82e9 \text{ (years)}$, the age of the universe in our model is increased by $\sim 2.14e9 \text{ (years)}$; therefore, reducing the discrepancy between the age of the oldest stars and that of the universe. For instance, HD140283 is one of the oldest known metal-deficient stars with estimated age of $14.46 \pm 0.8e9 \text{ (years)}$ which is believed to have been formed soon after the Big Bang [19]. Finally, the CMB redshift due to the expansion of space is found to be $z_x = 1068.29$. The gravitational redshifts at the hot and cold sides, on the

other hand, are found to be $z_{g_+} = 32.775$ and $z_{g_-} = 30.069$, respectively. The total redshift in the CMB dipole directions, therefore, is found to be $z_{xg_+} = 1101.07$ and $z_{xg_-} = 1098.36$, meeting the target gravitational redshift dipole $z_{g_+} - z_{g_-} = 2.70585$ and average redshift of $\bar{z}_{xg} = 1099.72$ (-).

9 Numerical simulation - supernovae type Ia

The plot of the apparent magnitude of the type Ia supernovae versus measured redshifts is called Hubble diagram. In this section, Hubble diagram obtained from the numerical simulation and its comparison with that of the observational data is discussed. In the numerical simulation, denoting the absolute luminosity of the sun L_{\odot} , we assume supernovae of various relative luminosities L/L_{\odot} occur in our model universe at various distances and orientations from the Milky Way. Then the resulting apparent magnitudes and the corresponding total redshifts z_{xg} are computed for the assumed distant supernovae. For a given absolute luminosity L , the higher the distance d_C , the higher the apparent magnitude m of the supernova (i.e. dimmer) and vice versa. To assess the validity of the model, the numerical predictions of the magnitudes versus redshifts are then compared against a large set of observational data presented in [17]. The observational data consists of the high redshift type Ia supernovae from Supernova Legacy Survey (SNLS) combined with mainly lower redshift data. This adds up to 472 data points (123 low- z , 93 SDSS, 242 SNLS and 14 HST). This large set of observational data can be downloaded from [18]. The overall numerical procedure for supernovae simulation is similar to that of the CMB dipole calculation. However, unlike the CMB radiation which is arriving from *equal* comoving distances all around, the supernovae occur at varying comoving distances d_C and orientations θ' . The latter is measured on the plane containing the primary direction and the Supernova. Fig 16a, shows the primordial comoving coordinate R_e of a *future* supernova in relation to the primordial coordinate R_o of the Milky Way and distance d_C from it. For a given angle θ' , knowing R_o and d_C the primordial coordinate R_e of the supernova is then obtained from:

$$R_e = \sqrt{R_o^2 + d_C^2 + 2R_o d_C \cos(\theta')} \quad (44)$$

Fig 16b, shows the universe expansion from the initial primordial condition of Fig 16a, to the scale factor a_e at the time t_e when the assumed supernova occurs and a beam of light leaves the emission point. While the light from the supernova explosion travels away from the emission point, as shown in Fig 16c, the universe continues expanding to the scale factor a_o when the light finally arrives at time t_o at the Milky Way with some total redshift z_{xg} . The physical distance cdt that light travels *immediately* after the supernova corresponds to the primordial comoving distance cdt/a_e away from the supernova, as shown in Fig's 16a,b. Integrating from the time of emission t_e to the time of observation t_o , we therefore have:

$$d_C = \int_{t_e}^{t_o} \frac{cdt}{a(t)} \quad (45)$$

Substituting in Eqn 45 for the scale factor $a(t)$ from Eqn 22 and integrating we then have:

$$d_C = (\sqrt{a(t_o)} - \sqrt{a(t_e)}) A \quad (46)$$

Alternatively, knowing the current epoch t_o and the comoving distance d_C to the supernova, the emission time t_e can be obtained from above as:

$$t_e = \{ [(\frac{3c}{A} t_o - 2)^{\frac{1}{3}} - \frac{d_C}{A}]^3 + 2 \} \frac{A}{3c} \quad (47)$$

The look-back time corresponding to the distance supernova is then simply given by $t_{lkbk} = t_o - t_e$. The farther the distance d_C , the smaller the time t_e and the deeper the look-back in time will be (closer to the Big Bang). The radiation *power* from the supernova explosion, received per unit area

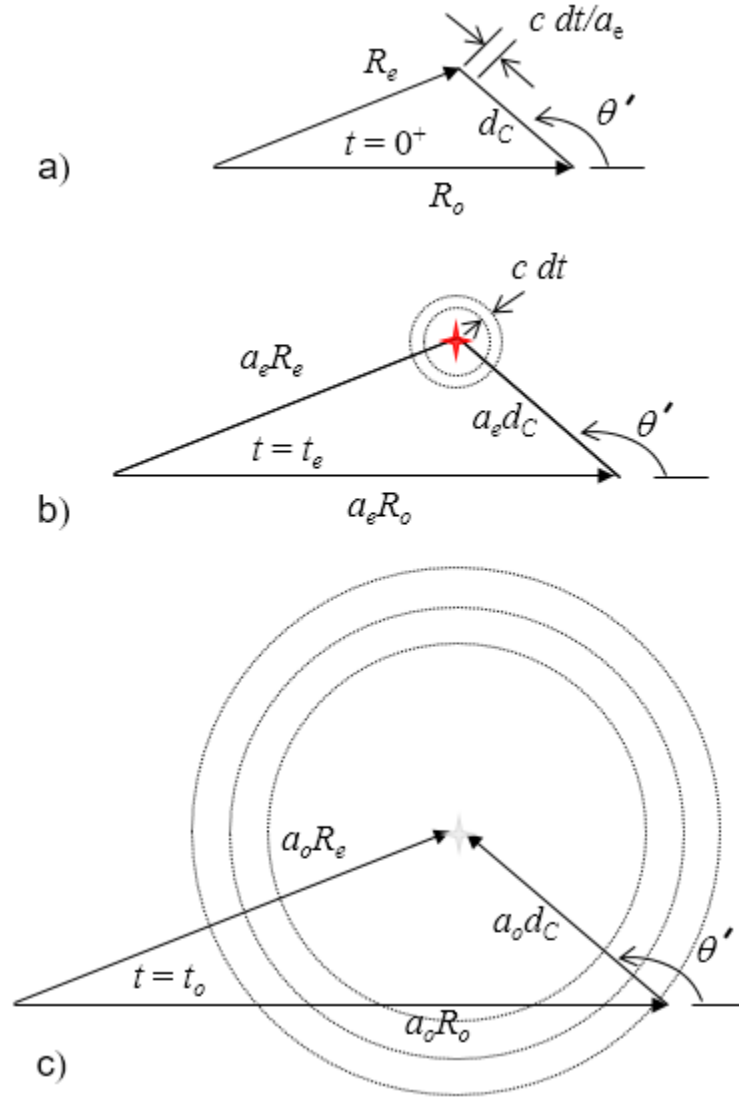


Figure 16: Comoving coordinates at the : a) primordial b) emission time c) observation time

at the Milky Way, is called the *apparent* luminosity l . The latter in terms of absolute luminosity L of the supernova, which in this article is expressed as multiples of solar power L_{\odot} , is given as [6]:

$$l = \frac{a_e^2}{4\pi a_o^4 d_C^2} L \quad (48)$$

Knowing the apparent luminosity from Eqn 48 the apparent magnitude m is calculated from [6]:

$$m = -2.5 \log_{10}(l) - 18.9965 \quad (49)$$

Note that for equation above the absolute luminosity L must be given in J/sec. Knowing t_o , R_o , d_C and θ' , first the current scale factor a_o , the primordial coordinate R_e and the emission time t_e of the supernova are obtained from Eqn's 22, 44 and 47, respectively. Then the scale factor a_e of the universe and the coordinate r_e of the supernova at the time of explosion are found from Eqns 22 and 27. For the assumed absolute luminosity L , then the apparent luminosity l is obtained using Eqn 48. Knowing the latter, the apparent magnitude m (needed for the Hubble diagram) is finally obtained from Eqn 49.

For calculation of the corresponding total redshift in the supernova's light, knowing both a_e and a_o , first the spatial expansion redshift z_x is obtained from Eqn 34. Knowing the PBH core size R_c from Eqn 18, the gravitational potentials Φ_o and Φ_e are then obtained from Eqn 35. The gravitational redshift z_g is then calculated from Eqn 36 and summed up with z_x to arrive at the total measurable redshift $z_{xg} = z_x + z_g$ of the light emitted from the supernova. The simulation then continues with a higher value of comoving d_C for all three directions in the simulation: $\theta' = \pi$ towards the singularity, $\theta' = 0$ away from it, or $\theta' = \pi/2$ normal to the primary direction. For

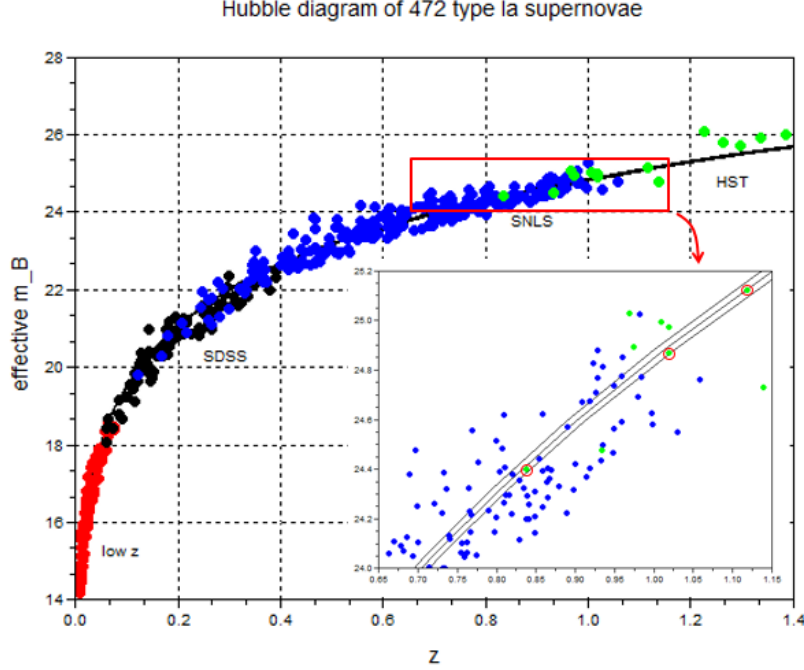


Figure 17: Hubble diagram - model versus observation

that reason, 3 curves are seen in the Hubble diagram. The upper curve corresponds to a case that light travels towards; and the lower curve corresponds to a case that light travels away from the singularity. The middle curve corresponds to a supernova whose line of sight is normal to the primary direction. At low redshifts the effect of gravitational anisotropy is small, and as such, three curves converge to each other. As the distance increases, the redshift anisotropy increases accordingly. At the comoving distance corresponding to that of the LSS, the *difference* between the upper and lower curves reaches to the maximum $g_{z+} - g_{z-} = 2.70585$; needed to satisfy the CMB dipole 3.35 (mK). In Fig 17, the resulting apparent magnitudes m versus their corresponding total redshifts z_{xg} are compared against the actual observations. The Hubble plot is obtained by adjusting the L/L_\odot such that *the number of supernova that fall within the band of anisotropy is maximized*. For example, as shown in the zoomed-in portion of Fig 17, there are 3 (out of 14) HST SN data points that fall within the band at such redshifts. The residual between the data and predictions is shown in Fig 18. For the latter, the SN that are within the band are compared with the middle curve, those that are above the upper curve are compared against the upper curve, and those that are below the lower curve are compared against the lower curve. Fig 19, shows the distribution of supernova count in each category as a function of the absolute luminosity of type Ia SN used in the simulations. By taking the solar luminosity as $L_\odot = 3.846e26$ (J/sec), the optimum SN count is achieved under type Ia SN absolute luminosity of $L^* = 3.02e9 \times L_\odot$, wherein 4 out of 123 Low z, 8 out of 93 SDSS, 27 out of 242 SNLS and 3 out of 14 HST data points fall within the band of anisotropy. This amounts to roughly 9% of the data points (i.e. 42 out of 472) for which absolute luminosity of the supernovae are found very comparable to each other. Let's call this set of supernovae the *Diamond set*, as listed in Fig 20. The remaining 91% of the type Ia SN in [17] have either higher (or lower) absolute luminosities; therefore, fall below (or above) the anisotropy

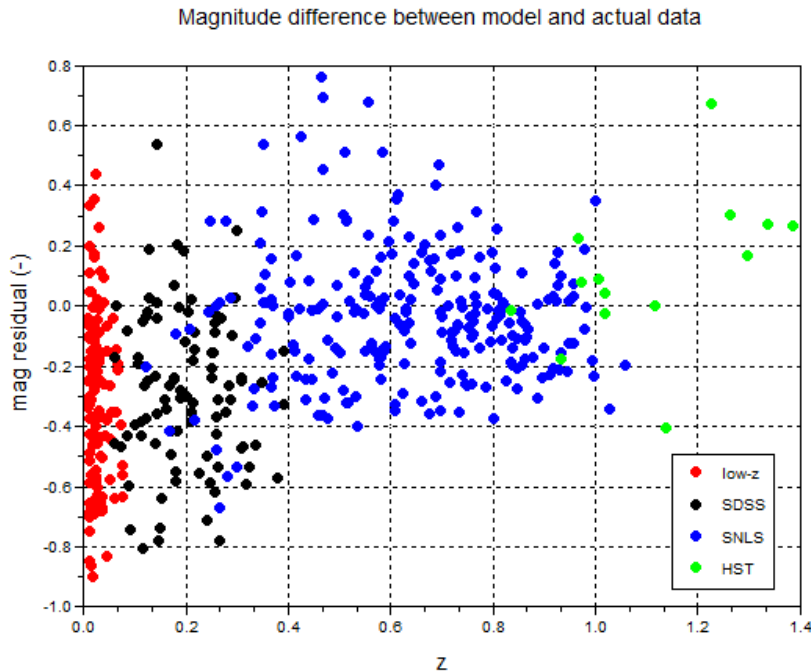


Figure 18: Residual (difference) between the actual data and predictions

band. Is this conclusion any plausible given that the type Ia supernovae are expected to be *standard candles with a fixed luminosity*? According to [16], there exists a significant *intrinsic* dispersion in the absolute magnitudes of the SN type Ia class *as a whole*. This implies that the progenitors of these events could be white dwarfs within the mass range $0.6 - 1.4M_{\odot}$ [20, 21] and/or variations in the explosion mechanisms. The uncertainty in the B-light magnitude of type Ia SN is determined be $\pm\Delta M \sim 0.8$ [16]. Knowing that the absolute magnitudes and the absolute luminosities (in units J/sec) are related through [6]:

$$M = -2.5 \log_{10}(L) + 71.2 \quad (50)$$

then the absolute magnitude of the Diamond set would be $M^* = -18.96$ and those of the entire 472 set could be within the range -18.96 ± 0.8 , therefore, $-18.16 < M < -19.76$. Using Eqn 50, then the absolute luminosities of the entire set of 472 supernovae could be within the range of $0.48 L^* < L < 2.09 L^*$, i.e. the range of x-axis used in generating Fig 19. Such range of absolute luminosities would bracket the entire set, as shown in Fig 21 in log scale for clarity. This, in turn, indicates that a best fit to such a large dispersion of the luminosity distribution (through minimizing the residuals of the entire set) could not be a reliable approach for constraining the model parameters, as it could improperly influence the selection of parameters. For that reason, the best fit in this work was obtained by *maximizing the number of SN count within the band of anisotropy*. In this exercise, the position of SN in relation to the primary direction was not taken into account.

An even more accurate way of using this model in determining L^* of type Ia supernovae, however, is first to use the *SN that are generally aligned with the CMB dipole*. For this, we propose having dedicated telescopes to those opposite directions and limited patches of the sky. Once an adequate number of data points are collected in those directions, then the best fit to the L^* could be obtained by minimizing the residuals of both the upper and lower curves. Once the L^* is determined more accurately (utilizing the information on both the magnitude and the direction of a SN), then a more comprehensive Diamond set could be determined using *all* the existing SN data, i.e. independent of their type, as long as they fall within the resulting well calibrated band of anisotropy. At that stage, the final validation of the theory might come when a *statistically significant* number of SN that happen to fall between the middle and upper curves are also found to be at the hot-CMB-pole

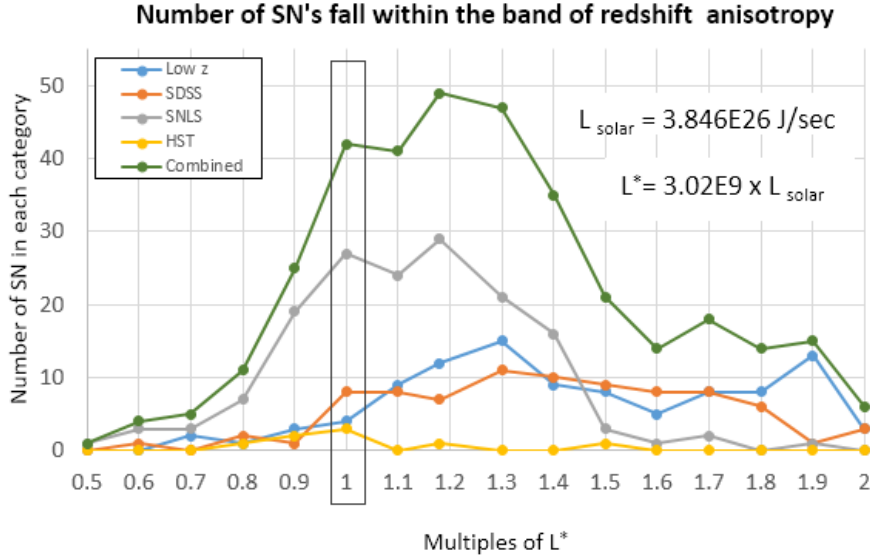


Figure 19: Absolute luminosity of type Ia SN best fit to the observational data

Lowz					
sn2006bq	sn2002de	sn2004as	sn2006bt		
SDSS					
SDSS6057	SDSS2992	SDSS5751	SDSS5103	SDSS6304	SDSS7847
SDSS8046	SDSS10550				
SNLS					
05D3mq	04D3ez	06D3fp	04D2cf	04D2gb	05D3lc
05D3mx	06D2ca	06D2ck	05D1cc	06D3et	05D3gp
04D1sa	05D1cb	03D4at	04D3cy	05D2le	04D2ja
04D3fq	04D1qd	04D4id	04D3lu	05D4dw	05D2by
05D2ay	04D1pd	05D3km			
HST					
2003eq	HST05FER	HST05Gab			

Figure 20: List of 42 type Ia SN with absolute luminosities $L^* = 3.02e9 \times L_{\odot}$

side of the sky; and similarly, those that happen to fall between the middle and lower curves are also statistically tend to be found at the opposite (cold-CMB-pole) side of the sky.

10 Hubble Constant

For the definitions of the Hubble constant and the critical energy density, in this section we have a very short review of the standard cosmological model. Considering the spherically symmetric nature of gravitational fields, the Friedman, Lemaitre, Robertson and Walker (FLRW) metric is defined as:

$$ds^2 = c^2 dt^2 - a^2(t) d\Sigma^2 \tag{51}$$

where the scale factor a is assumed to be a function of cosmic time t only; hence, inherently assuming a spatially homogeneous and isotropic properties for the universe in the standard cosmological model. The term $d\Sigma$ is the *comoving distance* defined as:

$$d\Sigma^2 = \frac{d\xi^2}{1 - k\xi^2} \xi^2 (d\theta^2 + \sin^2 \theta d\phi^2) \tag{52}$$

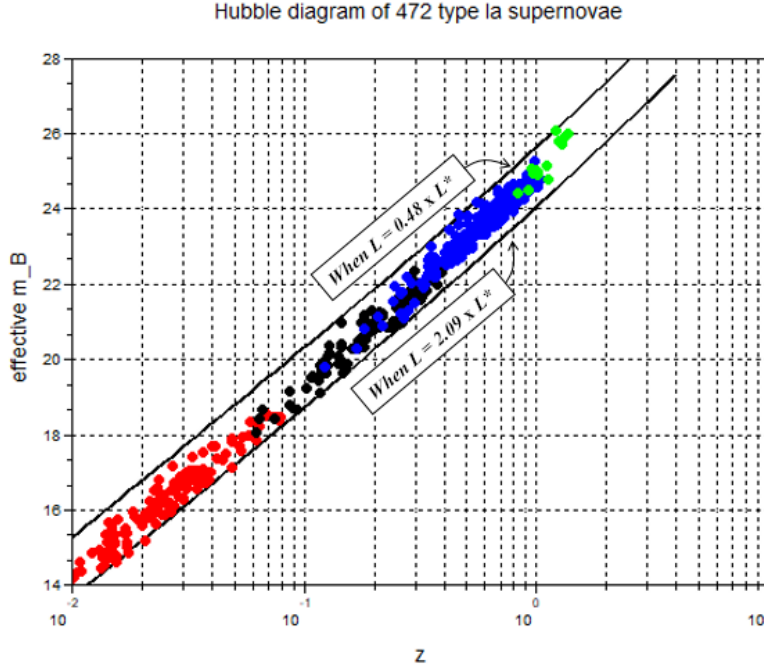


Figure 21: Upper and lower limits of absolute luminosity of type Ia SN

where $(d\xi, d\theta, d\phi)$ are the spatial intervals surrounding the comoving frame of any object in the universe and constant k is the Gaussian curvature of the space. The closed and open universes are obtained by $k = +1$ and $k = -1$, respectively, while a *flat* universe is given by $k = 0$. Using the FLRW metric and solving for the field equations of General Relativity, the equations of expansion, acceleration and energy density rate of the universe are given by Friedmann equations as follows [4]:

$$\begin{aligned}
 H^2 &= \left(\frac{\dot{a}}{a}\right)^2 = \frac{8\pi G}{3c^2} \rho - \frac{kc^2}{a^2} & (53) \\
 \frac{\ddot{a}}{a} &= -\frac{4\pi G}{3c^2} (\rho + 3p) \\
 \dot{\rho} &= -3H(\rho + p)
 \end{aligned}$$

Dividing both sides of the first equation above by H^2 we get:

$$1 = \frac{\rho}{\rho_c} - \frac{kc^2}{H^2 a^2} \quad (54)$$

where the critical *energy* density ρ_c of the universe is defined as:

$$\rho_c = \frac{3c^2 H^2}{8\pi G} \quad (55)$$

For a flat universe, where $k = 0$, from Eqn 54 we then must have $\rho = \rho_c$, i.e. the *energy density distribution in the universe must be equal to the critical value*. Finally, note that from $E = mc^2$, the relation between the mass density ρ_m and energy density ρ is given by:

$$\rho(t) = \rho_m(t)c^2 \quad (56)$$

Substituting for a and \dot{a} from Eqns 22 and 23 in the first Eqn 53 we arrive at the following equation for the Hubble constant H in our model:

$$H(t) = \frac{\dot{a}}{a} = \frac{2c}{3ct - 2A} \simeq \frac{2}{3t} \quad \dots \text{ for large } t \quad (57)$$

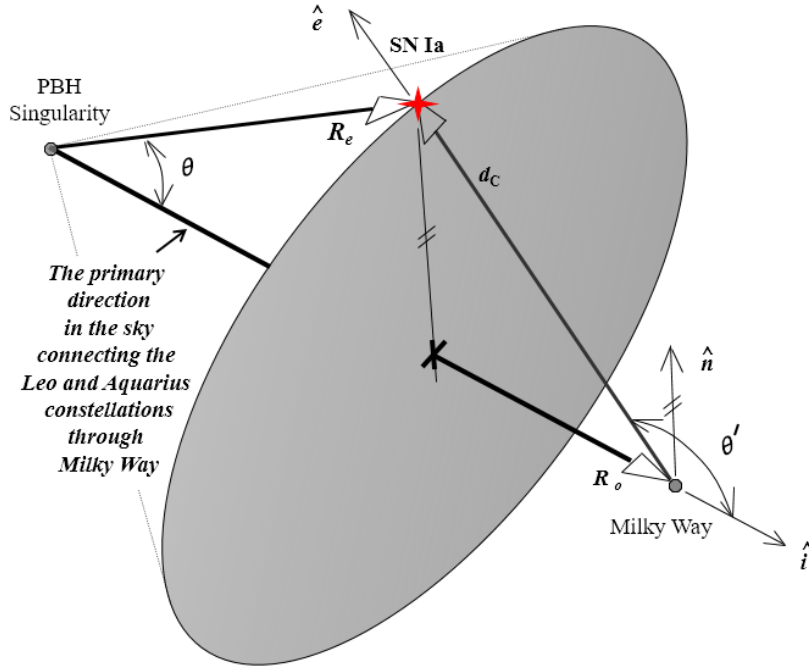


Figure 22: Primordial distance d_C of a SN in relation to the Milky Way and primary direction

The *dimensionless energy density parameter* Ω from the standard model is defined:

$$\Omega = \frac{\rho}{\rho_c} \quad (58)$$

In a close universe, $\Omega > 1$, the internal energy density is adequately high to eventually halt and then reverse the spatial expansion of the universe towards a big crunch. In an open universe, $\Omega < 1$, there is not adequate internal energy in the universe to prevent the run-away expansion originated from the Big Bang. In a flat universe, $\Omega = 1$, however, there is just about right amount of internal energy in the universe to *asymptotically halt the expansion*, hence, avoiding the re-collapse or run-away fates of the closed or open universes. Substituting for $\rho_m(t)$ from Eqn 33 in Eqn 56, the energy density versus time will be given as:

$$\rho(t) = \frac{3c^4}{2\pi GA^2} \frac{1}{a^3(t)} \quad (59)$$

Further, substituting for the energy densities ρ_c and $\rho(t)$ from Eqn's 55 and 59, respectively, in Eqn 58 we arrive at:

$$\Omega = \frac{4c^2}{H^2 A^2 a^3} \quad (60)$$

and then substituting for H and a from Eqn's 57 and 22, respectively, in Eqn 60 we finally arrive at:

$$\Omega = 1 \quad (61)$$

confirming *the inevitability of flat space under our cosmological model*. Knowing $t_o = 15.96e9$ (years), the current epoch energy density (which is also equal to the critical energy density of the universe) is found to be $\rho = \rho_c \sim 2.82e-10$ (J/m³). In comparison, the energy density of the PBH core (or black hole cores, in general) is $\rho_s \sim 1.23e38$ (J/m³).

11 Recession velocity of galaxies

To calculate the recession velocity of an emitting object relative to the Milky Way, the Hubble flow velocities \dot{r}_e and \dot{r}_o at the emission and observation points are calculated from Eqn 27 using their

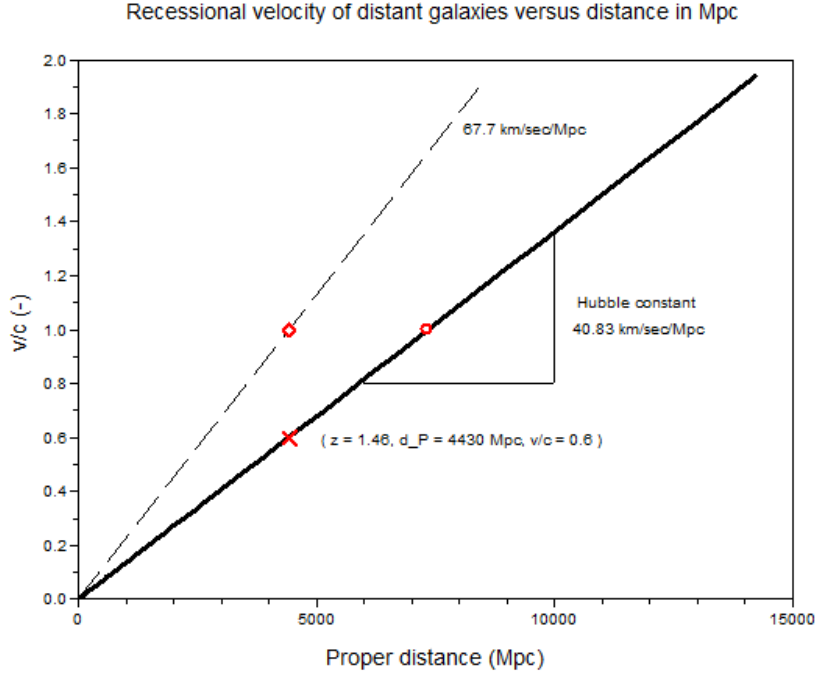


Figure 23: Hubble constant $H_o = 40.83$ from numerical simulation

corresponding cosmic times t_e and t_o , respectively. The recession velocity Δv along the vector \vec{d}_C is then obtained using:

$$\Delta v = \hat{e} \cdot \vec{r}_e - \hat{e} \cdot \vec{r}_o \quad (62)$$

where:

$$\begin{aligned} \vec{r}_o &= \dot{r}_o \hat{i} \\ \vec{r}_e &= \dot{r}_e \cos(\theta) \hat{i} + \dot{r}_e \sin(\theta) \hat{n} \\ \hat{e} &= \cos(\theta') \hat{i} + \sin(\theta') \hat{n} \end{aligned} \quad (63)$$

where the offset angle θ between the primary direction and R_e is calculated knowing:

$$R_e \sin(\theta) = d_C \sin(\theta') \quad (64)$$

The vectors \hat{i} and \hat{n} are the *unit vectors* along the primary direction and normal to it, respectively. These vectors are defined on the plane containing the singularity, the Milky Way and the emission point. The unit vector \hat{e} is along the line-of-sight of the emitting object, as illustrated in Fig 22.

Using these equations, the recession velocity Δv of the emitting object versus its proper distance d_P from the Milky Way is calculated and plotted in Fig 23 to arrive at the value of the Hubble constant $H_o = 40.83$ (km/sec/Mpc). Note on the graph that the recessional velocities of objects close to the observable horizon of the universe is approaching to $2c$, as had discussed before. According to the model, recessional velocity of the LSS is $v/c = 1.939$ at the proper distance 14236 (Mpc). Moreover, objects with a proper distance larger than $d_{su} \geq 7342$ (Mpc) have *superluminal* recession velocities (points to the right of the red circle on the black curve). Also according to the model, as shown in Fig 24, the *measurable* redshift of an object with the recessional velocity of $v/c = 1$ is in the range of $3.953 \leq z_{xg} \leq 4.038$, where the min and max values correspond to the hot and cold CMB pole directions, i.e. the black and blue curves, respectively. Contribution of the spatial expansion (the red dashed curve) to the measureable redshift in the superluminal case is $z_x = 3$ (the last point on the red curve). This was also illustrated earlier in Fig 6. The recessional velocity versus the entire range of measureable redshifts is shown in Fig 25. The superluminal recession velocity in

the standard cosmology [22], on the other hand, under generally accepted parameters $(\Omega_M, \Omega_\Lambda) = (0.3, 0.7)$, starts at measurable $z \geq 1.46$. In our model, the proper distance corresponding to such redshift is found to be $d_{su_standard_z} = 4430$ (Mpc). According to our model, an object with such redshift has $v/c \sim 0.6$, i.e. the red \times mark on Fig 23. However, in the standard model, an object in such distance (or redshift) has superluminal velocity $v/c = 1.0$, i.e. the red \diamond on the Figure, which results in the misestimated Hubble constant of $c/d_{su_standard_z} = 67.7$ (km/sec/Mpc), in line with the current estimates of the Hubble constant in the literature. According to our model, therefore, the current estimate of the Hubble constant from the standard model could be overestimated by a factor of $\frac{1.0}{0.6}$, i.e. by $\sim 66\%$.

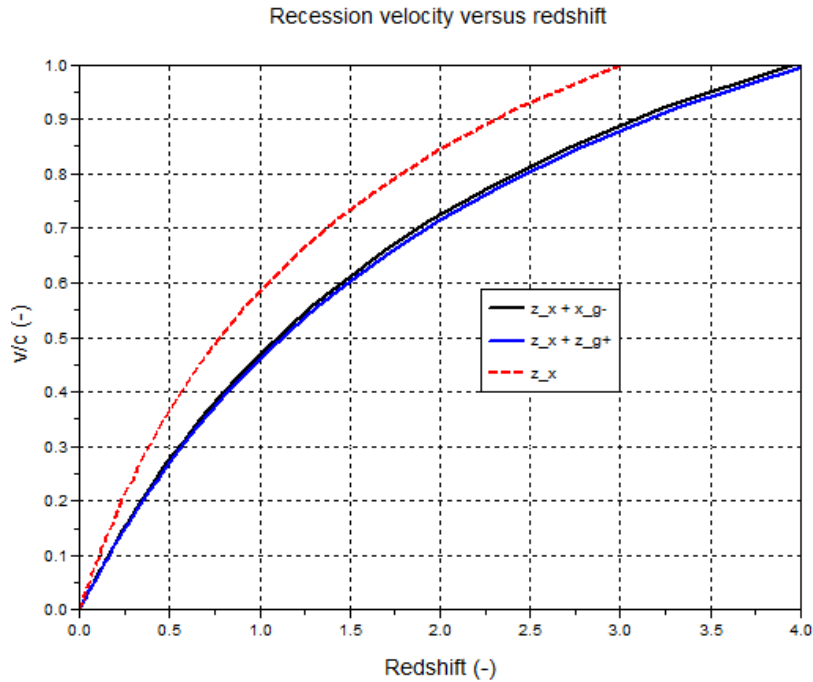


Figure 24: Recession velocity of objects in the low range of z

12 Conclusion

A cosmological model is introduced wherein the universe is in a condensed steady state condition prior to its expansion at the Big Bang. The steady state condition represents the state of the core of a primordial super-massive black hole in this theory. At the Big Bang, velocity of the concentric spherical shells of the primordial condensation change from initial value zero to the speed of light c - relative to their local rest frames - within one cosmological time step A/c . The work done on the condensation increases the core temperature by some 50 orders of magnitude; i.e. from its initial value in the range $30.009e-34 - 1.167e-34$ (K) to post Big Bang temperature of $2.13e16$ (K). Immediately after the Big Bang the universe begins to decelerate. The known universe was shown to be the observable part of a much bigger structure - named the grand universe. It was shown that the CMB dipole of amplitude 3.35 mK could be due to the gravitational redshift anisotropy caused by the matter residing beyond the horizon of the observable universe. The gravitational redshift of CMB is found to be $z_{g_CMB} > 30(-)$. The measureable redshift was shown to be made of the superposition of the gravitational and spatial redshifts. The Hubble diagram constructed using the numerical simulation of the apparent magnitudes and the measureable redshifts of type Ia SN was compared against a large set of observational data. The best fit to the data was found when type Ia SN absolute luminosity L^* was taken to be $3.02e9$ times that of the sun L_\odot . The age of the universe was found to be $15.96e9$ (years), i.e. $\sim 2.14e9$ (years) older than that of the standard cosmology.

The recombination time was found to be 456600 (years) after the Big Bang. The actual value of the Hubble constant was found to be 40.83 (km/sec/Mpc). The discrepancy with the current estimated range of 67 – 71 (km/sec/Mpc) is partly due to neglecting the gravitational redshifts of the grand universe in the standard cosmology.

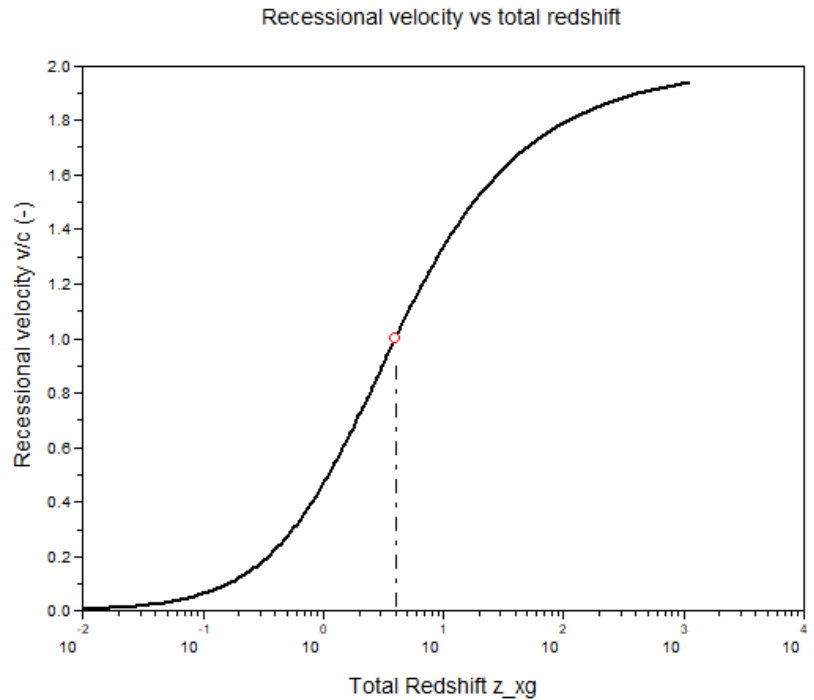


Figure 25: Recession velocity of objects in the entire range of z

References

- [1] F. Abrari, 'Combined theory of Special Relativity and Quantum Mechanics', <https://viXra.org/abs/2106.0167>
- [2] B. J. Carr, 'Primordial Black Holes - Recent Developments', 22nd Texas Symposium, Stanford, 12-17 Dec 2004, arXiv:astro-ph/0505034v1 1 Apr 2005
- [3] A. Guth, 'MIT opencourseware', Lecture 7 - Dynamics of Homogeneous expansion part III, <https://youtube/m00PjHTq6jU>
- [4] A. Friedmann, On the curvature of space, General relativity and gravitation, 31 (12): 1991-2000
- [5] Gravitational field and potential, <http://astrowww.phys.uvic.ca/tatum/celmechs/celm5.pdf>
- [6] S. Weinberg, Gravitation and cosmology, Wiley, 1972
- [7] D. W. Hogg, Distance measures in cosmology, Astrophysics, 9905116 v4 , 16 Dec 2000
- [8] R.C. Tolman, Relativity, thermodynamics and cosmology, Dover publications, New York 2016
- [9] K. Schwarzschild, Uber das gravitationsfeld eines massenpunktes nach der Einsteinschen theorie, 1916, Sitzungsberichte der deutschen akademie der wissenschaften zu Berlin, pp 189
- [10] A.G. Riess et. al., 'Type Ia Supernova discoveries at $z > 1$ from Hubble Space Telescope: evidence for past deceleration and constraints on dark energy evolution astro-ph/0402512v2/March 200

- [11] B. J. Carr, 'Primordial Black Holes - Recent Developments', 22nd Texas Symposium, Stanford, 12-17 Dec 2004, arXiv:astro-ph/0505034v1 1 Apr 2005
- [12] A. Kogut et. a., 'Dipole anisotropy in COBE-DMR first year sky maps', 1993, ApJ, 419,1
- [13] M. Jaroszynski et. al., 'The cosmic microwave background dipole cannot be the result of the cosmological entropy gradient', 1995, ApJ, 448:448-493
- [14] T. Lauer and M. Postman, 'The motion of the local group with respect to the 15,000 km/sec Abell cluster internal frame', 1994, ApJ, 425:418-438
- [15] https://maps.gsfc.nasa.gov/mission/observatory_cal.html, Page updated 04/16/2010
- [16] M.M. Phillips, 'The absolute magnitudes of type Ia supernovae', 1993, The Astrophysical Journal, 413:L105-L108
- [17] A. Conley et. al. , 'Supernova constraints and systematic uncertainties from the first three years of supernova legacy survey', The Astrophysical Journal Supplement Series, 2011, 192:1-29
- [18] <https://tspace.library.utoronto.ca/handle/1807/25390>, University of Toronto
- [19] H.E. Bond, et. al. 'HD 140283: A star in the solar neighborhood that formed shortly after the Big Bang', The Astrophysical Journal Letters, 765 (1):L12
- [20] T. Shigeyama et. al. 'Possible models for the type Ia supernova', 1992, The Astrophysical Journal Letters, 386, L13
- [21] S.E. Woosley and T.A. Weaver, 'Sub-Chandrasekhar mass modes for type Ia supernovae', 1994, ApJ, 423, 371
- [22] T. M. Davis and C. H. Lineweavers, 'Superluminal recession velocities', 2001, arXiv:astro-ph/0011070v2
- [23] https://www.esa.int/ESA_Multimedia/Images/2013/03/Planck_cosmic_recipe, ESA
- [24] A. Einstein and W. de Sitter, 'On the relation between the expansion and the mean density of the universe' Proceedings of the National Academy of Science, 18 (3): 213-214, 1932
- [25] D.L. Edwin and E.J.Spillar, 'A measurement of the mass density of the universe', ApJ, 307:L1-L4, 1986
- [26] F. Abrari, 'Quantum description of Newtonian gravity', <https://vixra.org/abs/2107/0004>